Carbon Trends 12 (2023) 100285

Contents lists available at ScienceDirect

Carbon Trends

journal homepage: www.elsevier.com/locate/cartre

One-step synthesis of Co_3O_4 nanoparticles/laser induced graphene composites in ambient condition for electrocatalytic OER reaction

Jiangli Li [a], Xue Yu [a], Rongke Sun [a], Hao Li [a], Xiaodong Zhu [a], Yanqing Ma [a,b,*], Lei Ma [a,**]

[a] Tianjin International Center for Nanoparticles and Nanosystems, Tianjin University, 92 Weijin Road, Nankai District, Tianjin 300072, PR China
[b] School of Precision Instrument and Opto-electronics Engineering, Tianjin University 300072, PR China

ARTICLE INFO

Keywords:
Basswood
Co_3O_4 nanoparticles
Graphene composites
Laser induced one-step synthesis
Electrocatalysis
Oxygen evolution reaction

ABSTRACT

In this paper, we report a successful one-step synthesis of Co_3O_4 Nanoparticles/Laser induced graphene (NPs/LIG) composite by using 1064 nm laser with irradiating cobalt salts impregnated basswood slices in air. The prepared Co_3O_4 NPs/LIG composites show uniformly distributed nanoparticles on the high-quality 3D graphene. It can be directly used as working electrode for electrochemical reactions without the need for extra post-treatment and exhibits remarkable performance for electrocatalytic OER reaction with an overvoltage of 325 mV at current density of 10 mA·cm^{-2} and Tafel slope of 66.63 mV·dec^{-1}. Due to its great capability of fabrication precision, simplicity and high speed, this technique indicates immense potential in large scale electrochemical micro-sensor manufacture.

1. Introduction

Graphene has been extensively studied with a broad spectrum of applications in energy storage [1–4], electronics [5,6], sensing [7,8] and other fields [9,10] because of its large specific surface area, outstanding electric, thermal conductivity and mechanical properties [11–15]. Considering these excellent properties of graphene, their composite material made with metal or metal oxide may own some dreamed catalytic properties in industry [16–18], especially for electrocatalytic OER reaction [19,20]. Although, IrO_2 and RuO_2 system indicate outstanding OER catalytic effect, their high costs largely limit their potential in real applications [21,22]. Hence, intensive works have been conducted to seek the alternative cheap transition metal oxides [23] and their composites, such as nickel oxide/graphene, iron oxide/graphene [24,25] and cobalt oxide/graphene [26]. Especially, the Co_3O_4/graphene catalysts have been intensively investigated [27–29] since Co_3O_4 has the highest stability among all cobalt oxides and its graphene-based composites have an outstanding OER activeness. Song et al. [30] reported an excellent OER catalytic performance under alkaline conditions of an ultra-thin Co_3O_4/rGO (reduced Graphene Oxide) nanocomposite synthesized using hydrothermal method. It overpotential was 290 mV which is far less than that of bare Co_3O_4 catalyst. Later, a Co_3O_4 decorated reduced rGO nano electrode showed an ultra-low starting potential of 1.38 V with current density of 10 mA/mg [28]. However, in all above studies, the preparation of Co_3O_4/graphene composites requires to multiple steps of graphene oxide synthesis, metal oxides nanoparticles deposition, and reduction of graphene [31], which are normally complicated and time consuming with using quite amount of non-recyclable chemicals [32–34].

While, laser induced graphene (LIG) [35,36] technology has been proved to be an effective and low-cost method for producing high-quality graphene, which can easily achieve macroscopic LIG with controllable morphology and high porosity [37,38]. With the development of LIG technology, the preparation of MO/LIG composite materials through laser induced one-step synthesis method is considered promising. Dan Xu et al. [39] reported successful synthesis of ultra-small sized Cu_xO nanoparticles on a porous laser induced graphene, which is formed by irritating laser on PI (Polyimide) layer on a piece of foam nickel with spin coated $CuCl_2$. Ruquan Ye et al. [40] created metal oxide nanoparticles embedded in porous Graphene in situ by directly laser scribing on polyimide (MC-PI) films containing metal complexes. But polyimide or other polymers are expensive and will pollute the environment. Biomass materials have the advantages of abundant sources, low cost, rich carbon content, and three-dimensional pore structure, making them

* Corresponding author at: Tianjin International Center for Nanoparticles and Nanosystems, Tianjin University, 92 Weijin Road, Nankai District, Tianjin 300072, PR China.
** Corresponding author.
E-mail addresses: mayanqing@tju.edu.cn (Y. Ma), Lei.ma@tju.edu.cn (L. Ma).

https://doi.org/10.1016/j.cartre.2023.100285
Received 11 June 2023; Received in revised form 12 July 2023; Accepted 12 July 2023
Available online 13 July 2023

a substitute for polymers [41–43]. Xiao Han et al. succeeded in converting metal nitride solution soaked cedar wood into graphene embedded with Ni, Fe, Cu, Co and NiFe nanocrystals through CO_2 laser scribing [44]. Libei Huang et al. [45] demonstrated that naturally occurring wood can be engineered into a miniaturized LIG materials water treatment system by laser engraving. However, there are currently few studies on the one-step synthesis of MO/biomass based LIG through laser induction.

Here, we present a newly developed simple methodology for one-step synthesizing Co_3O_4 nanoparticles/laser induced graphene (Co_3O_4 NPs/LIG) composites out of cobalt salt solution socked basswood chips by irritation of 1064 nm laser under an ambient condition without any inner gas protection. Basswood-based LIG maintains the original three-dimensional pore structure of biomass materials, which is conducive to the loading of nanoparticles, and Co_3O_4 nanoparticles in Co_3O_4 NPs/LIG are uniformly dispersed on the surface of LIG. The choice of basswood is attributed to its original high porosity with high concentration of lignocellulose [46,47]. It has unique straight channel and layered porous structure which can facilitate the absorption of metal salts. Besides, it is rich in hydroxyl groups that can coordinate with metal ions [48,49]. Further investigation was conducted on the OER catalytic performance of different Co_3O_4 NPs/LIG composite catalysts synthesized. This method has good guiding significance for the preparation of MO/LIG catalysts and the design of catalytic based sensors.

2. Results and discussion

2.1. Preparation of Co_3O_4 NPs/LIG composites

As shown in Fig. 1, MO NPs/LIG (where MO stands for metal oxide) is fabricated by laser-induced one-step synthesis under ambient condition in air. In order to introduce the targeting metallic atom, basswood slices were initially soaked in metal nitrate solvent. The lignocellulose contains abundant hydroxyl functional groups that can evenly anchor metal cations through electrostatic interaction and coordination bonds, consequently, offering a favorable condition for uniform metal oxides loading. 1064 nm laser pulses were focused to the surface of metal salt-soaked basswood. The laser-spot burst heat would directly convert lignocellulose into graphene, and oxidize metal cations into metal oxides. Compared with basswood without metal salt, laser irritation could result instant burning in the air due to the violent reactions between the graphitic substance of wood and oxygen (Fig. S1). In our design, metal salt impregnation make basswood darker which further enhances the laser absorption. Therefore, in air, only a fractional energy of laser pulses is used to convert MO NPs/LIG. The obtained MO NPs/LIG can be directly used for electrochemical working electrode through precise packaging without post-treatment.

2.2. Characterization of Co_3O_4 NPs/LIG composites

It is clearly seen that basswood has a 3D porous structure composed of multiple large channels (50–70 μm) and multiple small channels (10–20 μm) as shown in Fig. 2a. After laser irritation in air, the solid skeleton of basswood changes into a fluffy structure, forming a loosely stacked layered structure which is demonstrated as Fig. 2b. The close-up view of skeleton shows a gauze-like covering with uniformly distributed nanoparticles of an average particle size about 500 nm, as shown in Fig. 2c. The energy dispersive X-ray spectrum (EDX), as shown in Fig. 2d, indicates that the main elements of composites prepared by laser irritation are C, O and Co with uniform distribution. Furthermore, the composite was analyzed using X-ray diffraction (XRD). Six diffraction peaks at 19 °, 31.4 °, 36.8 °, 44.9 °, 59.5 ° and 65.3 ° are present which could be attributed to the four main crystal planes of cubic Co_3O_4 (PDF#76–1802), demonstrating the successful synthesis of crystalline Co_3O_4 [50]. There is a small diffraction peak at 26.1 °, which corresponds to the (002) plane of carbon material [51]. It shows that the surface of basswood is carbonized and Co_3O_4 nanoparticles are formed at the same time (Fig. 2e). Raman spectroscopy (Raman) was further used to analyze the chemical structure of basswood impregnated with cobalt nitrate before and after laser irritation showing in Fig. 2f. Without laser irritation, the Raman spectrum of basswood is featureless, however, after laser irritation, it shows typical graphene D, G and 2D bands at 1350, 1580 and 2700 cm^{-1}, corresponding to the disordered defect structure of graphene, the stretching of C—C bond in graphene and the second-order two-phonon process of graphene sp^2, respectively [52,53]. This proves the formation of graphene through laser irradiation. Furthermore, in the same spectrum, peaks around 190, 472, 512, 604, and 676 cm^{-1} corresponds the $^3F_{2g}$, E_g, $^2F_{2g}$, $^1F_{2g}$, and A_{1g} Raman-active modes of Co_3O_4, respectively [54,55], indicating the formation of spinel cobalt tetroxide particles decorated graphene, which highly coincide with the XRD measurements.

In order to analyze the surface chemical state of Co_3O_4 NPs/LIG composite in detail, X-ray photoelectron spectroscopy (XPS) measurements were conducted. The fine spectra of C and Co elements are shown in Fig. 2g and 2h. C 1s is composed of four peaks, with binding energy (BE) of 283.75, 284.6, 285.65 and 287.37 eV, respectively, corresponding to C—C sp^2 bond, C—C sp^3 bond, C—OH bond and C = O bond [56,57] (Fig. 2g). The smaller peak area ratio of carboxyl group (C = O) (13.5) and the larger peak area ratio of C—C (58.5) indicate that the carbonization degree of two-dimensional and three-dimensional carbon on the surface of basswood is significantly improved after laser irritation [52,57]. As shown in Fig. 2h, the main peaks with binding energy of

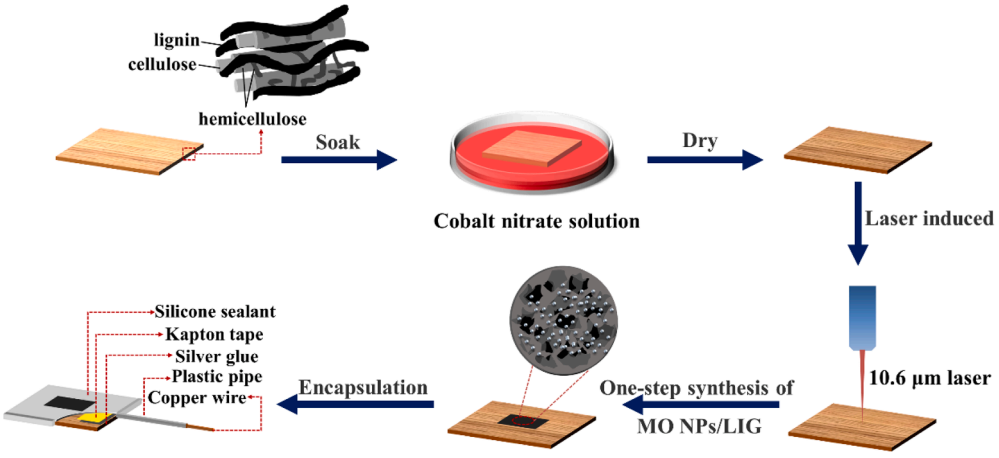

Fig. 1. Schematic diagram of preparation and packaging of the electrode made of Co_3O_4 NPs/LIG composite.

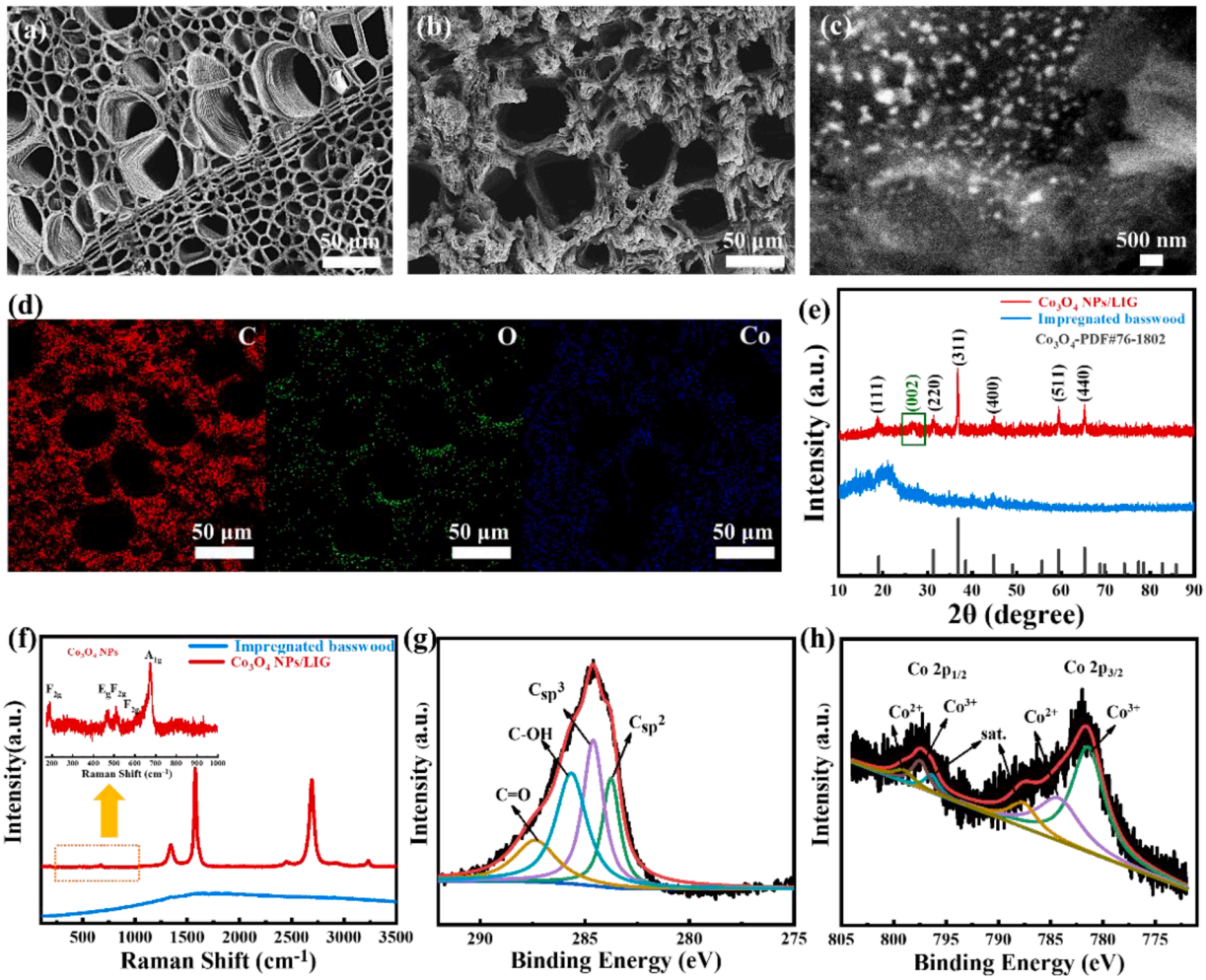

Fig. 2. (a)-(b) SEM images of basswood impregnated with cobalt nitrate before and after laser irritation; (c) A close-up view of fluffy structure; (d) Element mapping of the laser induced composite materials; (e)-(f) XRD and Raman characterization of basswood impregnated with cobalt nitrate before and after laser irritation; (g)-(h) C, O element analysis of XPS spectrum of the laser-induced one-step synthesized composites.

797.2 eV and 781.8 eV are displayed in the Co 2p region, which can be attributed to $2p_{1/2}$ and $2p_{3/2}$, respectively [58]. The energy change of about 15 eV between $2p_{1/2}$ and $2p_{3/2}$ indicates the presence of divalent and trivalent Co species in the Co_3O_4 spinel. Detailed analysis shows that 781.6 eV and 784.5 eV are from Co^{3+} and Co^{2+} of Co $2p_{3/2}$ respectively, and the ratio of $Co^{2+}$and $Co^{3+}$is close to 1:2 [54]. Again, all the above

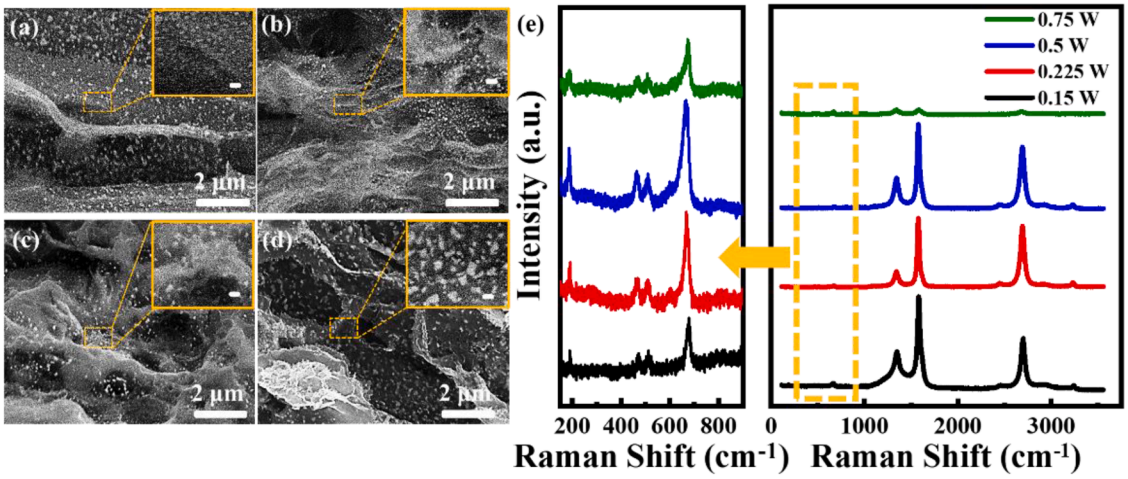

Fig. 3. (a)-(d) SEM of Co_3O_4 NPs/LIG prepared under different laser power of 0.15 W, 0.225 W, 0.5 W and 0.75 W, the scale of inset close-up is 300 nm; (e)Raman spectra of Co_3O_4 NPs/LIGs prepared under different laser power conditions. The left plot shows the Raman spectra of Co_3O_4 in wavenumber between150 and 900 cm^{-1} that is the close-up of the yellow dashed frame circled in the right plot.

measurements proved that Co_3O_4 NPs/LIG was successfully prepared by laser-induced one-step synthesis in air.

2.3. Effect of laser parameters on the synthesized Co_3O_4 NPs/LIG composites

In order to explore the influence of laser power, Co_3O_4 NPs/LIG composite materials were prepared using different laser power (0.15, 0.225, 0.5 and 0.75 W). The morphology of composites was shown in Fig. 3a-d. When the laser power is 0.15 W, the nanoparticles on the surface of the carbon support material are relatively flat and the blocky of carbon support material in the composite, shown as the enlarged view. As shown in Fig. 3b, when the laser power is further increased to 0.225 W, the surface of product is presented as an ultra-thin mesh with uniformly covered small sized nanoparticles. When the laser power is further increased to 0.5 W, the composite exhibits a thick flower shape covered with slightly larger nanoparticles on the surface. As the laser power reaching 0.75 W, the composite surface mainly shows agglomeration nanoparticles and collapsed carbon support carrier. The Raman characterization of composite materials prepared under different laser power conditions is shown in Fig. 3e. On the left side of Fig. 3e is a close-up of the spectra from150 to 900 cm^{-1} (yellow dotted box), they clearly show the featured Raman peaks of Co_3O_4 [54,55]. The intensity of the featured Raman peaks of Co_3O_4 increase with the increase of laser power, and the $^3F_{2g}$ of Co_3O_4 in the composite material become prominent when the laser power higher than 0.225 W, as well as the gradually improved graphene quality reflected by the decreased I_D/I_G and increased I_{2D}/I_G showing in Fig. 3e and Fig. S2, respectively [52,53]. Continuously rising the power to 0.75 W, the featured Raman peak start to become weaker, while the deterioration of grown LIG starts at the laser power of 0.5 W [59,60]. Due to the laser pulse irritation, a rapid energy accumulation and much slower heat dissipation on the interaction area leads the extremely high temperatures on the surface of basswood, consequently, an instant carbonization and graphitization accompanying with fast flaking processes caused by the quick expansion of laser spot interacted area will facilitate the formation of LIG [61]. When the laser power is further increased, great biomass fibers damage is unavoidable, consequently, the diminishing their structural integrity and the material carving on the surface. The laser power dependent results indicate that 0.225 W laser power is the optimal condition for forming a composite covered by high quality with uniformly dispersed small size nanoparticles. Excessive laser power can lead to the collapse of carbon support materials and the sintering of nanoparticles [61,62].

Moreover, the effect of laser scanning speed (LSS) on the graphitization of LIG and the size distribution of Co_3O_4 nanoparticles was further investigated (Fig. S3). When the LSS is 500 mm/s, only a little amount of tulle material appeared (Fig. S3a). Lowering the scanning speed could increase the laser beam dwelling time at each point therefore irritate more energy at each spot, resulting in more damage to the fiber and higher porosity in the fiber [63]. With the speeding up laser scanning, more thin gauze like materials were produced (Fig. S3b-f). From the Raman graph in Fig. S3g, it can also be seen that the material prepared at 500 mm/s is amorphous carbon, with only a weak G peak. However, with the increase of LSS, the featured Raman peaks of graphene show up and maximized at LSS of 1000 mm/s. Further the Raman characteristic peaks of graphene gradually weaken. Because the scanning speed is too fast to having enough time for carbonization [54]. For nanoparticles, the size and number of nanoparticles decreases with the increase of scanning speed [64,65], and higher LSS is not conducive to the preparation of nanoparticles (Fig. S4). When the scanning speed is too high, the interaction time between the laser beam and the material will be too short, which may not be sufficient for the growth of metal oxide nanoparticles [66].

Additionally, the number of laser processing cycles (NLPC) have significant effects on the morphology of the formed Co_3O_4 NPs/LIG as shown in Fig. S5. Specifically, when the NLPC is 4, although much graphene had been synthesized which is identified by the Raman results, but almost no signal of Co_3O_4 nanoparticles was observed. Continuously rising the NLPC, the amount of graphene reticulates increases, and the observable signal of Co_3O_4 nanoparticles start to appear at the NLPC of 6. When the NLPC is up to 10, the amount of gauze-like thin materials increases significantly and reaches the maximum with a large number of uniformly distributed nanoparticles on them (Fig. 5f). However, further rising the NLPC, the gauze-like thin materials start to decrease and completely disappear at the NLPC of 12 which can be interpreted as oxidation reaction between the graphitic material in air triggered by the energy irritated by the laser [67]. The exactly same trend was reproduced as the intensity change of Raman 2D peak. Hence, laser power, LSS, and the NLPC are the three key parameters to determine the quality LIG and both the size and spatial distribution of surface decorated metal oxide nanoparticles [39,61]. The optimal conditions are 0.225 W of laser power, 1000 mm/s of LSS and 10 of NLPC.

The effect of metal salt concentration on the morphology and size of the composite were further investigated. The Co_3O_4 NPs/LIG composite was prepared by laser irritation out of cobalt nitrate solvents soak basswood at the concentration of 0.1 M, 0.5 M and 1 M. When the concentration of cobalt nitrate is 0.1 M, the most of the yielded composite materials are bare biomass skeleton of basswood with only fractional coverage by gauze like material and few nanoparticles (Fig. 4a and 4d). For the concentration of cobalt nitrate of 0.5 M, the surface of the composite material was fully covered with the gauze like materials (Fig. 4b) with a large number of uniformly distributed small sized nanoparticles (Fig. 4e). When increasing the concentration of cobalt nitrate to 1 M, some flocculent materials and coalesced nanoparticles appear on the surface of the composite material as shown in Fig. 4c [68,69].

2.4. Study on electrochemical properties of Co_3O_4 NPs/LIG composites

The OER performance tests were carried out using Co_3O_4 NPs/LIG composite as a working electrode. The electrocatalytic activity of four different samples, 0.1 M Co_3O_4 NPs/LIG, 0.5 M Co_3O_4 NPs/LIG, 1 M Co_3O_4 NPs/LIG and LIG electrodes (0.1 M, 0.5 M, and 1 M represent the cobalt nitrate concentration of impregnated basswood wood), were studied in alkaline electrolyte solution (1 M KOH) at room temperature. The electrochemical performance of the OER of the four samples was evaluated by recording the relation between overpotential and RHE at a fixed current. As shown in Fig. 5a, the overpotential for 0.1 M Co_3O_4 NPs/LIG, 0.5 M Co_3O_4 NPs/LIG, 1 M Co_3O_4 NPs/LIG and LIG at a current density of 10 $mA{\cdot}cm^{-2}$ are 423 mV, 325 mV, 388 mV and 637 mV, respectively. The electrodes were prepared using only LIG requires a high overpotential of 637 mV, indicating that LIG has very low OER catalytic activity. Compared to the bare LIG, there are some nanoparticles on the surface of 0.1 M Co_3O_4/LIG, which makes its catalytic activity superior to that of LIG. 0.5 M Co_3O_4 NPs/LIG exhibits a lower overpotential than 0.1 M Co_3O_4 NP/LIG, but further increasing the cobalt nitrate concentration to 1 M, the higher overpotential required for 1 M Co_3O_4 NP/LIG to reach the same current density. Composite made of 1 M Co_3O_4 NPs/LIG shows largely reduced electrochemical activity due to the seriously active sites blocking caused by the aggregated surface nanoparticles. Whereas, for 0.5 M Co_3O_4 NPs/LIG, there are small amount of uniformly dispersed nanoparticles on the surface of the LIG, which can expose more metal oxide active sites and lead to better catalytic activity [70]. Moreover, the large surface area and high conductivity provided by LIG can improve mass transfer and expand the electrode/electrolyte contact area, thereby improving OER activity [71,72]. To further evaluate its OER performance, the Tafel slope was fitted giving an approximate 66.63 $mV{\cdot}dec^{-1}$ which was smaller than that of 0.1 M Co_3O_4 NPs/LIG (98.11 $mV{\cdot}dec^{-1}$), 1 M Co_3O_4 NPs/LIG (72.13 $mV{\cdot}dec^{-1}$), and LIG (104.86 $mV{\cdot}dec^{-1}$) (Fig. 5b). This signals the fast current increases than potential which makes its superior surface reaction kinetics that all others [73,74].

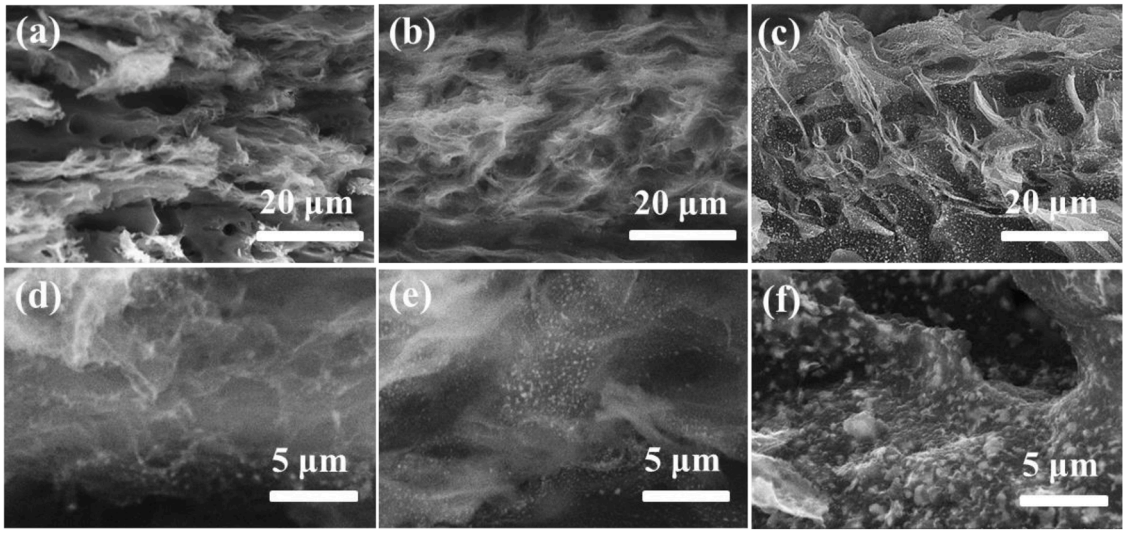

Fig. 4. (a)-(c) SEM images of laser induced one-step synthesis of Co_3O_4 NPs/LIG composites after drying basswood soaked in cobalt nitrate solvents with concentrations of 0.1 M, 0.5 M, and 1 M; (d)-(f) The corresponding close-up of SEM images.

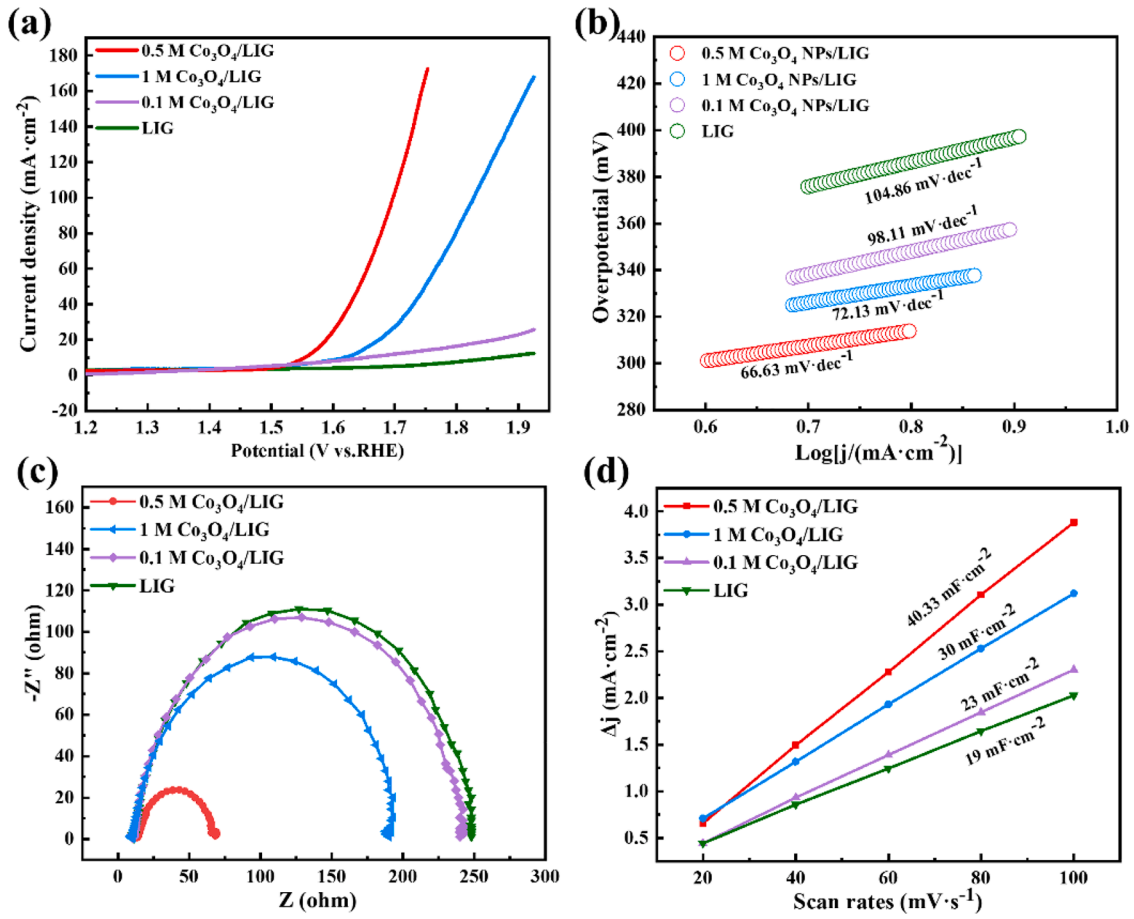

Fig. 5. Comparison of OER electrochemical activities of 0.1 M Co_3O_4 NPs/LIG, 0.5 M Co_3O_4 NPs/LIG, 1 M Co_3O_4 NPs/LIG and LIG electrodes in 1 M KOH: (a) linear sweep voltammetry curve, (b) Tafel diagram, (c) Nyquist diagram by fitting Randle circuit, and (d) specific activity diagram by ECSA normalization curve.

The role of electrode dynamics of these electrodes in the OER process was investigated by electrochemical impedance spectroscopy (EIS) measurement in the frequency range of 10 mHz to 100 kHz with the open circuit voltage, which gives the interface reaction charge transfer resistance (R_{ct}) of these electrodes in 1 M KOH electrolyte solution. The Nyquist curve is shown in Fig. 5c, compared to 0.1 M Co_3O_4 NPs/LIG (110 Ω), 1 M Co_3O_4 NPs/LIG (90 Ω), and LIG (120 Ω), the minimum charge transfer resistance (28 Ω) was observed in 0.5 M Co_3O_4 NPs/LIG composites which indicates its faster charge transfer rate and lower energy barrier during OER than the sample made in other conditions.

The low R_{ct} reveals that the introduction of Co_3O_4 NPs without agglomeration on the high-quality LIG can greatly improve electron transfer rate in the OER process [75,76]. Since the number of active sites is related to the electrochemical active surface area (ECSA), an electrochemical double layer capacitance (C_{dl}) was adopted to analyze ECSA (Fig. 5e and Fig. S6). Compared to the C_{dl} of 0.1 M Co_3O_4 NPs/LIG (23 mF·cm^{-2}), 1 M Co_3O_4 NPs/LIG (30 mF·cm^{-2}) and LIG (19 mF·cm^{-2}), the 0.5 M Co_3O_4 NP/LIG has the highest C_{dl} of 40.33 mF·cm^{-2}, indicating it has the most available active sites on the surface structure of 0.5 M Co_3O_4 NP/LIG [77] and which coincides its excellent OER catalytic performance (see Table S1 to compare the OER performance of different cobalt-based catalysts prepared by different methods).

3. Conclusion

In summary, Co_3O_4 NPs/LIG composites were successfully prepared by laser induced one-step synthesis. As an OER electrode, it has excellent electrocatalytic performance, under the current density of 10 mA·cm^{-2}, the required overpotential is 325 mV, and the Tafel slope is 66.63 mV·dec^{-1}. Due to its great capability of fabrication precision, simplicity, low cost and high speed, this technique embryos immense potential in large scale electrochemical micro-sensor manufacture.

4. Methods

4.1. Materials synthesis

Cut into 5 × 5 × 2 mm^3 thin slices along the direction perpendicular to the growth of basswood, and dried at 60 ℃ after ultrasonic washing. Dissolve cobalt nitrate hexahydrate in deionized water to prepare 0.1 M, 0.5 M and 1 M cobalt nitrate solutions. Immersing the basswood slices in cobalt nitrate solution for 24 h, washing off excessive nitrate on the surface, and drying them in an oven at 80 ℃ for 12 h before taking them out. Laser irritation was then conducted on the metal-complex-containing basswood slices with a 1064 nm laser engraving system (Sundor KF-30 L with a pulse duration of 10 μs) under ambient condition. The power of the laser is 30 W (0.1%−100% adjustable).

When investigating the laser power parameters on the fabricate materials, the laser power was set to 0.15 W, 0.225 W, 0.5 W, and 0.75 W. The LSS was 1000 mm/s, the NLPC was 10, and the metal salt concentration was 0.5 M.

When investigating the LSS, Co_3O_4 NPs/LIGs were prepared at speeds of 500 mm/s, 1000 mm/s, 1500 mm/s, 2000 mm/s, 2500 mm/s, and 3000 mm/s. The laser power was 0.25 W, the NLPC was 10, and the metal salt concentration was 0.5 M.

When dependence of the NLPC on the fabricated materials, Co_3O_4 NPs/LIGs were prepared at 4, 6, 8, 10, and 12 cycles with a laser power of 0.25 W, a LSS of 1000 mm/s, and a metal salt concentration of 0.5 M.

4.2. Characterization

The surface morphology of the samples was characterized by scanning electron microscopy (SEM, Hitachi, SU-3500). Energy dispersive X-ray spectroscopy (EDS, IXRF system, SU-3500) was used to characterize the elements and their distributions. The Raman spectra used Raman spectrometer (ANDOR-MARZHAUSER) with a 532 nm laser and the power was about 2 mW on the objects. The X-ray photoelectron spectroscopy (XPS, Thermo Scientific, ESCALAB 250Xi) was used to analyze surficial constituents. The binding energies were extracted according to the calibrated C 1 s line at 284.6 eV.

X-ray diffraction (XRD, Dandong Tongda Technology, TD-3500) characterizations were carried out to analyze the crystallinity and lattice constants of samples.

4.3. Electrochemical characterization

For OER measurements, the back of Co_3O_4 NPs/LIG electrodes ware coated with silver paint and sealed by a Kapton tape so that the silver glue and attached copper wire can be isolated from the electrolyte during electrochemical test, showing in Fig. S1. The LSV and EIS studies of OER were conducted in a self-made electrochemical cell, where the Hg/HgO electrode and Pt electrode were chosen as the reference and counter electrode, respectively. Electrochemical impedance spectroscopy (EIS) measurements were carried out in the frequency range of 10 mHz to 100 kHz with open circuit voltage by a CHI 760E electrochemical workstation. The CV curves were measured at different scanning speeds (20–100 mV·s^{-1}), and then the scanning speed (mV·s^{-1}) is plotted by taking the difference of its corresponding current density (mA·cm^{-2}) under a fixed voltage where the slope of the fitting line is C_{dl}. For the Hg/HgO electrode, E (RHE)=E (Hg/HgO)+0.098+0.0592×pH.

CRediT authorship contribution statement

Jiangli Li: Investigation, Data curation, Methodology, Writing – original draft. **Xue Yu:** Data curation, Methodology. **Rongke Sun:** Data curation. **Hao Li:** Methodology. **Xiaodong Zhu:** Methodology. **Yanqing Ma:** Supervision, Data curation, Methodology, Writing – review & editing. **Lei Ma:** Conceptualization, Visualization, Investigation, Supervision, Data curation, Funding acquisition, Methodology, Writing – review & editing.

Declaration of Competing Interest

The authors declare that they have no known competing financial interests or personal relationships that could have appeared to influence the work reported in this paper.

Acknowledgments

The National Key R&D Program of China (No. 2020YFC2004602).

Supplementary materials

Supplementary material associated with this article can be found, in the online version, at doi:10.1016/j.cartre.2023.100285.

References

[1] Z.M. Ren, J.Y. Di, Z.K. Lei, R. Mao, Fabrication and performance test of flexible supercapacitors based on three-dimensional graphene hydrogel, Mater. Sci. Forum 1058 (2022) 45–50.
[2] X. Zhang, M. Zhao, Z.J. Chen, T. Yan, J.L. Li, Y.Q. Ma, L. Ma, The application of biomass-based carbon materials in flexible all-solid supercapacitors, J. Mater. Sci. Mater. Electron. 33 (2022) 15422–15432.
[3] J.Y. Zhu, L.X. Wang, X.M. Gan, T.T. Tang, F.W. Qin, W.X. Luo, Q.Q. Li, N.N. Guo, S. Zhang, D.Z. Jia, H.H. Song, Graphene quantum dot inlaid carbon nanofibers: revealing the edge activity for ultrahigh rate pseudocapacitive energy storage, Energy Storage Mater. 47 (2022) 158–166.
[4] A. Poorna, R. Saravanathamizhan, N. Balasubramanian, Graphene and graphene-like structure from biomass for electrochemical energy storage application-a review, Electrochem. Sci. Adv. 1 (2021) 1–16.
[5] K.M. Zhang, P.X. Ji, J. Zhao, D.X. Yang, M. Zhao, Z.Z. Zhang, G. Liu, L. Ma, Low contact resistance side-interconnects strategy for epi-graphene based electronic integration, J. Mater. Sci. Mater. Electron. 33 (2022) 17249–17257.
[6] V. Saraswat, R.M. Jacobberger, M.S. Arnold, Materials science challenges to graphene nanoribbon electronics, ACS Nano 15 (2021) 3674–3708.
[7] C.M. Li, J.Q. Wu, H.Y. Shi, Z.Y. Xia, J.K. Sahoo, J.J. Yeo, D.L. Kaplan, Fiber-based biopolymer processing as a route toward sustainability, Adv. Mater. 34 (2022) 1–27.
[8] S. Han, C. Liu, N. Li, S.D. Zhang, Y.P. Song, L.Q. Chen, M. Xi, X.L. Yu, W.B. Wang, M.G. Kong, One-step fabrication of nitrogen-doped laser-induced graphene derived from melamine/polyimide for enhanced flexible supercapacitors, CrystEngComm 24 (2022) 1866–1876.
[9] Y.L. Zhao, X.Y. Wang, X.M. Guo, N. Shi, D.D. Cheng, H. Zhou, N. Saito, T.X. Fan, Nitrogen-doped 3D porous graphene coupled with densely distributed CoO_x

nanoparticles for efficient multifunctional electrocatalysis and Zn-Air battery, Electrochim. Acta 420 (2022) 1432–1440.
[10] F.R. Fan, R.X. Wang, H. Zhang, W.Z. Wu, Emerging beyond-graphene elemental 2D materials for energy and catalysis applications, Chem. Soc. Rev. 50 (2021) 10983–11031.
[11] C. Cervetti, A. Rettori, M.G. Pini, A. Cornia, A. Repollés, F. Luis, M. Dressel, S. Rauschenbach, K. Kern, M. Burghard, The classical and quantum dynamics of molecular spins on graphene, Nat. Mater. 15 (2016) 164–172.
[12] C. Berger, Z. Song, T.B. Li, X.B. Li, A.Y. Ogbazghi, R. Feng, Z.T. Dai, A. N. Marchenkov, E.H. Conrad, P.N. First, Ultrathin epitaxial graphite: 2D electron gas properties and a route toward graphene-based nanoelectronics, J. Phys. Chem. B 108 (2004) 19912–19916.
[13] C. Liu, Z.H. Li, R.X. Qiao, Q.H. Wang, Z.B. Zhang, F. Liu, Z.Q. Zhou, N.Z. Shang, H. W. Fang, M.X. Wang, Z.K. Liu, Z. Feng, Y. Cheng, H. Wu, D.W. Gong, S. Liu, Z. S. Zhang, D.X. Zou, Y. Fu, J. He, H. Hong, M.H. Wu, P. Gao, P.H. Tan, X.Q. Wang, D.P. Yu, E.G. Wang, Z.J. Wang, K.H. Liu, Designed growth of large bilayer graphene with arbitrary twist angles, Nat. Mater. 21 (2022) 1263–1269.
[14] T. Tan, Z.Y. Yuan, H. Zhang, G.F. Yan, S.Y. Zhou, N. An, B. Peng, G. Soavi, Y.J. Rao, B.C. Yao, Multispecies and individual gas molecule detection using Stokes solitons in a graphene over-modal microresonator, Nat. Commun. 12 (2021) 6716–6722.
[15] A. Kurzmann, Y. Kleeorin, C.Y. Tong, R. Garreis, A. Knothe, M. Eich, C. Mittag, C. Gold, F.K. de Vries, K. Watanabe, T. Taniguchi, V. Fal'ko, Y. Meir, T. Ihn, K. Ensslin, Kondo effect and spin-orbit coupling in graphene quantum dots, Nat. Commun. 12 (2021) 1–6.
[16] X.H. Tian, Y.K. Zhou, B.Y. Zhang, N.B.S. Selabi, G.R. Wang, Monodisperse polar $NiCo_2O_4$ nanoparticles decorated porous graphene aerogel for high-performance lithium sulfur battery, J. Energy Chem. 74 (2022) 239–251.
[17] K.F. Zhang, J. Qiu, J. Wu, Y.Q. Deng, Y.H. Wu, L.F. Yan, Morphological tuning engineering of Pt@TiO_2/graphene catalysts with optimal active surfaces of support for boosting catalytic performance for methanol oxidation, J. Mater. Chem. A Mater. Energy Sustain. 10 (2022) 4254–4265.
[18] Y. Sushma, C. Maruf, J. Mercykutty, M. Priti, Distinguished performance of biogenically synthesized reduced-graphene-oxide-based mesoporous Au-Cu_2O/rGO ternary nanocomposites for sonocatalytic reduction of nitrophenols in water, New J. Chem. 46 (2022) 9685–9694.
[19] W.H. Fang, J. Wang, Y. Hu, X.Q. Cui, Z.X. Li, Metal-organic framework derived Fe-Co-CN/reduced graphene oxide for efficient HER and OER, Electrochim. Acta 365 (2021) 1–12.
[20] Z.K. Ghouri, K. Elsaid, M.M Nasef, A. Badreldin, Y. Wubulikasimu, A. Abdel-Wahab, Incorporation of manganese carbonyl sulfide ($(Mn_2S_2(CO)_7)$ and mixed metal oxides-decorated reduced graphene oxide ($MnFeCoO_4$/rGO) as a selective anode toward efficient OER from seawater splitting under neutral pH conditions, Renew. Energy 190 (2022) 1029–1040.
[21] T. Reier, I. Weidinger, P. Hildebrandt, R. Kraehnert, P. Strasser, Electrocatalytic oxygen evolution reaction on iridium oxide model film catalysts: influence of oxide type and catalyst substrate interactions, in: Proceedings of the 224th ECS Meeting, 2013, pp. 39–51.
[22] H.C. Ma, C.P. Liu, J.H. Liao, Y. Su, X.Z. Xue, W. Xing, Study of ruthenium oxide catalyst for electrocatalytic performance in oxygen evolution, J. Mol. Catal. Chem. 247 (2006) 7–13.
[23] X. Yu, C.W. Hu, P.X. Ji, L. Ma, Optically transparent ultrathin NiCo alloy oxide film: precise oxygen vacancy modulation and control for enhanced electrocatalysis of water oxidation, Appl. Catal. B Environ. Int. J. Devoted Catal. Sci. Appl. 310 (2022) 1–13.
[24] R.Y. Fan, J.Y. Xie, N. Yu, Y.M. Chai, B. Dong, Interface design and composition regulation of cobalt-based electrocatalysts for oxygen evolution reaction, Int. J. Hydrog. Energy 47 (2022) 10547–10572.
[25] W.C. Wan, S.Q. Wei, J.G. Li, C.A. Triana, Y. Zhou, G.R. Patzke, Transition metal electrocatalysts encapsulated into N-doped carbon nanotubes on reduced graphene oxide nanosheets: efficient water splitting through synergistic effects, J. Mater. Chem. A 7 (2019) 15145–15155.
[26] J.Y. Xu, J.J. Li, D.H. Xiong, B.S. Zhang, Y.F. Liu, K.H. Wu, I. Amorim, W. Li, L. F. Liu, Trends in activity for the oxygen evolution reaction on transition metal (M = Fe, Co, Ni) phosphide pre-catalysts, Chem. Sci. 9 (2018) 3470–3476.
[27] J.H. Zhang, F. Li, W.B. Chen, C.S. Wang, D.D. Cai, Facile synthesis of hollow Co_3O_4-embedded carbon/reduced graphene oxides nanocomposites for use as efficient electrocatalysts in oxygen evolution reaction, Electrochim. Acta 300 (2019) 123–130.
[28] A.V. Munde, B.B. Mulik, R.P. Dighole, B.R. Sathe, Cobalt oxide nanoparticles decorated reduced graphene oxide (Co_3O_4-rGO): active and sustainable nanoelectrodes for water oxidation reaction, New J. Chem. 36 (2020) 1–14.
[29] Z. Zhu, J. Zhang, X. Peng, Y. Liu, D. Yuan, Co_3O_4-$NiCo_2O_4$ hybrid nanoparticles anchored on N-doped reduced graphene oxide nanosheets as an efficient catalyst for Zn-Air batteries, Energy Fuels 35 (2021) 4550–4558.
[30] Y.F. Song, Y.Y. Chen, J. Hu, H.L. Diao, W.J. Luo, Facile preparation of ultrathin Co_3O_4/nanocarbons composites with greatly improved surface activity as high efficient OER catalyst, Chemistry 23 (2017) 4010–4016. Easton.
[31] R. Ye, J.M. Tour, Graphene at fifteen, ACS Nano 13 (2019) 10872–10878.
[32] X. Gao, L.M. Zheng, F. Luo, J. Qian, J.Y. Wang, M.Z. Yan, W.D. Wang, Q.C. Wu, J. C. Tang, Y.S. Cao, C.W. Tan, J.L. Tang, M.J. Zhu, Y.N. Wang, Y.L. Li, L.Z. Sun, G. H. Gao, J.B. Yin, L. Lin, Z.F. Liu, S.Q. Qin, H.L. Peng, Integrated wafer-scale ultra-flat graphene by gradient surface energy modulation, Nat. Commun. 13 (2022) 1–16.
[33] Z.K. Zhang, J.H. Du, D.D. Zhang, H.D. Sun, L.C. Yin, L.P. Ma, J.S. Chen, D.G. Ma, H. M. Cheng, W.C. Ren, Rosin-enabled ultraclean and damage-free transfer of graphene for large-area flexible organic light-emitting diodes, Nat. Commun. 8 (2017) 1–9.
[34] Z. Chen, W. Ren, L. Gao, B. Liu, S. Pei, H.M. Cheng, Three-dimensional flexible and conductive interconnected graphene networks grown by chemical vapour deposition, Nat. Mater. 10 (2011) 424–428.
[35] Z.C. Zhang, M.M. Song, J.X. Hao, K.B. Wu, C.Y. Li, C.G. Hu, Visible light laser-induced graphene from phenolic resin: a new approach for directly writing graphene-based electrochemical devices on various substrates, Carbon N Y 127 (2018) 287–296.
[36] Y. Chyan, R.Q. Ye, Y.L. Li, S.P. Singh, C.J. Arnusch, J.M. Tour, Laser-induced graphene by multiple lasing: toward electronics on cloth, paper, and food, ACS Nano 12 (2018) 2176–2183.
[37] L.B. Huang, L. Ling, J.J. Su, Y. Song, Z.Y. Wang, B.Z. Tang, P. Westerhoff, R.Q. Ye, Laser-engineered graphene on wood enables efficient antibacterial, anti-salt-fouling, and lipophilic-matter-rejection solar evaporation, ACS Appl. Mater. Interfaces 12 (2020) 51864–51872.
[38] R. Trusovas, K. Ratautas, G. Raciukaitis, G. Niaura, Graphene layer formation in pinewood by nanosecond and picosecond laser irradiation, Appl. Surf. Sci. 471 (2019) 154–161.
[39] D. Xu, K.C. Chan, H.J. Guo, H. Zhong, L. Lu, One-step fabrication of a laser-induced forward transfer graphene/Cu_xO nanocomposite-based electrocatalyst to promote hydrogen evolution reaction, J. Mater. Chem. A 9 (2021) 16470–16478.
[40] R.Q. Ye, Z.W. Peng, T. Wang, Y.N. Xu, J.B. Zhang, Y.L. Li, L.G. Nilewski, J. Lin, J. M. Tour, *In situ* formation of metal oxide nanocrystals embedded in laser-induced graphene, ACS Nano 9 (2015) 9244–9251.
[41] Y.J. Kim, T. Le, D. Son, H.K. Nam, D.W. Yang, B. Kim, Wood-based flexible graphene thermistor with an ultra-high sensitivity enabled by ultraviolet femtosecond laser pulses, Cirp Annals-Manufacturing Technology 70 (2021) 443–446.
[42] G.F. Hawes, D. Yilman, B.S. Noremberg, M.A. Pope, Supercapacitors fabricated via laser-induced carbonization of biomass-derived poly(furfuryl alcohol)/graphene oxide composites, ACS Appl. Nano Mater. 2 (2019) 6312–6324.
[43] S. Yu, L. Wang, Q. Li, Y. Zhang, H. Zhou, Sustainable carbon materials from the pyrolysis of lignocellulosic biomass, Mater. Today Sustain. 19 (2022) 1–12.
[44] X. Han, R.Q. Ye, Y. Chyan, T. Wang, C.H. Zhang, L.L. Shi, T. Zhang, Y. Zhao, J. M. Tour, Laser-induced graphene from wood impregnated with metal salts and use in electrocatalysis, Acs Appl. Nano Mater. 1 (2018) 5053–5061.
[45] L.B. Huang, L. Ling, J.J. Su, Y. Song, Z.Y. Wang, B.Z. Tang, P. Westerhoff, R.Q. Ye, Laser-engineered graphene on wood enables efficient antibacterial, anti-salt-fouling, and lipophilic-matter-rejection solar evaporation, ACS Appl. Mater. Interfaces 12 (2020) 51864–51872.
[46] W.T. Gan, L.P. Wu, Y.X. Wang, H. Gao, L.K. Gao, S.L. Xiao, J.Q. Liu, Y.J. Xie, T. Li, J. Li, Carbonized wood decorated with cobalt-nickel binary nanoparticles as a low-cost and efficient electrode for water splitting, Adv. Funct. Mater. 31 (2021) 1–10.
[47] T. Shui, M.F. Pan, Y. Lu, J.W. Zhang, Q.X. Liu, P.A. Nikrityuk, T. Tang, Q. Liu, H. B. Zeng, High-efficiency and durable removal of water-in-heavy oil emulsions enabled by delignified and carboxylated basswood with zwitterionic nanohydrogel coatings, J. Colloid Interface Sci. 612 (2022) 445–458.
[48] H.S. Yaddanapudi, K. Tian, S. Teng, A. Tiwari, Facile preparation of nickel/carbonized wood nanocomposite for environmentally friendly supercapacitor electrodes, Sci. Rep. 6 (2016) 1–9.
[49] R. Miller, T. Debroy, Energy absorption by metal-vapor-dominated plasma during carbon dioxide laser welding of steels, J. Appl. Phys. 68 (1990) 2045–2050.
[50] L.H. Liu, M. Yang, S. Gao, X.F. Zhang, X.L. Cheng, Y.M. Xu, H. Zhao, L.H. Huo, Co_3O_4 hollow nanosphere-decorated graphene sheets for H_2S sensing near room temperature, ACS Appl. Nano Mater. 2 (2019) 5409–5419.
[51] C.N. Barnakov, G.P. Khokhlova, A.N. Popova, S.A. Sozinov, Z.R. Ismagilov, XRD characterization of the structure of graphites and carbon materials obtained by the low-temperature graphitization of coal tar pitch, Eurasian Chem. Technol. J. 17 (2015) 87–92.
[52] J. Lin, Z.W. Peng, Y.Y. Liu, F. Ruiz-Zepeda, R.Q. Ye, E.L.G. Samuel, M.J. Yacaman, B.I. Yakobson, J.M. Tour, Laser-induced porous graphene films from commercial polymers, Nat. Commun. 5 (2014) 5714–5721.
[53] R.Q. Ye, Y. Chyan, J.B. Zhang, Y.L. Li, X. Han, C. Kittrell, J.M. Tour, Laser-induced graphene formation on wood, Adv. Mater. 29 (2017) 1–7.
[54] Z.L. Wu, L.P. Sun, M. Yang, L.H. Huo, H. Zhao, J.C. Grenier, Facile synthesis and excellent electrochemical performance of reduced graphene oxide-Co_3O_4 yolk-shell nanocages as a catalyst for oxygen evolution reaction, J. Mater. Chem. A 4 (2016) 13534–13542.
[55] Z.F. Mahdi, R.A. Faris, Z.S. Sadeq, Fast, sensitive and low-cost chemical sensor based on manufacturing nanostructured Co_3O_4 using Raman spectroscopy, Nano Struct. Nano Objects 28 (2021) 1–5.
[56] L. Stobinski, B. Lesiak, A. Malolepszy, M. Mazurkiewicz, B. Mierzwa, J. Zemek, P. Jiricek, I. Bieloshapka, Graphene oxide and reduced graphene oxide studied by the XRD, TEM and electron spectroscopy methods, J. Electron. Spectros. Relat Phenom. 195 (2014) 145–154.
[57] R. Al-Gaashani, A. Najjar, Y. Zakaria, S. Mansour, M.A. Atieh, XPS and structural studies of high quality graphene oxide and reduced graphene oxide prepared by different chemical oxidation methods, Ceram. Int. 45 (2019) 14439–14448.
[58] T. Liu, L.Y. Zhang, W. You, J.G. Yu, Core-shell nitrogen-doped carbon hollow spheres/Co_3O_4 nanosheets as advanced electrode for high-performance supercapacitor, Small 14 (2018) 407–414.
[59] A.C. Ferrari, J.C. Meyer, V. Scardaci, C. Casiraghi, M. Lazzeri, F. Mauri, S. Piscanec, D. Jiang, K.S. Novoselov, S. Roth, Raman spectrum of graphene and graphene layers, Phys. Rev. Lett. 97 (2006) 1–4.

[60] A.C. Ferrari, D.M. Basko, Raman spectroscopy as a versatile tool for studying the properties of graphene, Nat. Nanotechnol. 8 (2013) 235–246.
[61] M. Liu, J.N. Wu, H.Y. Cheng, Effects of laser processing parameters on properties of laser-induced graphene by irradiating CO_2 laser on polyimide, Sci. China Technol. Sci. 65 (2022) 41–52.
[62] W.T. Wang, L.S. Lu, Y.X. Xie, W.B. Wu, R.X. Liang, Z.H. Li, Y. Tang, Controlling the laser induction and cutting process on polyimide films for kirigami-inspired supercapacitor applications, Sci. China: Technol. Sci. 64 (2021) 651–661.
[63] Y.H. Yen, C.S. Hsu, Z.Y. Lei, H.J. Wang, C.Y. Su, C.L. Dai, Y.C. Tsai, Laser-induced graphene stretchable strain sensor with vertical and parallel patterns, Micromachines (Basel) 13 (2022) 1–14.
[64] A. Ziefuss, S. Barcikowski, L.V. Zhigilei, Advances in pulsed laser synthesis of nanoparticles in liquids, Sci. China Phys. Mech. Astron. 65 (2022) 1–24.
[65] A. Nyabadza, M. Vazquez, B. Fitzpatrick, D. Brabazon, Effect of liquid medium and laser processing parameters on the fabrication of carbon nanoparticles via pulsed laser ablation in liquid towards paper electronics, Colloids Surf. Physicochem. Eng. Asp. 636 (2022) 1–7.
[66] B. Kulyk, B.F.R. Silva, A.F. Carvalho, A.J.S. Fernandes, F.M. Costa, E. Fortunato, M. Matos, D.V. Evtuguin, Conversion of paper and xylan into laser-induced graphene for environmentally friendly sensors, Diam. Relat. Mater. 123 (2022) 1–8.
[67] K. Sinha, L.J. Meng, Q.W. Xu, X.H. Wang, Laser induction of graphene onto lignin-upgraded flexible polymer matrix, Mater. Lett. 286 (2021) 1–4.
[68] S. Gyawali, L.K.M.O. Goni, M.S. Chowdhury, A. Laref, S. Bajgai, S. Chantrapromma, K. Techato, Effect of KOH concentration on the properties of ZnO nanoparticles, Mater. Res. Express 9 (2022) 1–6.
[69] K. Heydaryan, M.A. Kashi, A.H. Montazer, Tuning specifc loss power of $CoFe_2O_4$ nanoparticles by changing surfactant concentration in a combined co-precipitation and thermal decomposition method, Ceram. Int. 12 (2022) 16967–16976.
[70] S.R. Xu, Y.S. Du, X. Yu, Z. Wang, X.H. Cheng, Q. Liu, Y.L. Luo, X.P. Sun, Q. Wu, A Cr-FeOOH@Ni-P/NF binder-free electrode as an excellent oxygen evolution reaction electrocatalyst, Nanoscale 13 (2021) 17003–17010.
[71] Y.D. Ma, H. Zhang, J. Xia, Z.R. Pan, X.F. Wang, G. Zhu, B. Zheng, G.X. Liu, L. M. Lang, Reduced $CoFe_2O_4$ /graphene composite with rich oxygen vacancies as a high efficient electrocatalyst for oxygen evolution reaction, Int. J. Hydrog. Energy 45 (2020) 11052–11061.
[72] Y.F. Ma, W.H. Chen, Z.Q. Jiang, X.N. Tian, G. Wang, X. Yi, G.L. Chen, Z.J. Jiang, NiFe nanoparticles supported on N-doped graphene hollow spheres entangled with self-grown N-doped carbon nanotubes for liquid electrolyte/flexible all-solid-state rechargeable zinc-air batteries, J. Mater. Chem. A 10 (2022) 12616–12631.
[73] R. Sanchis Gual, A. Seijas Da Silva, M. Coronado Puchau, T.F. Otero, G. Abellan, E. Coronado, Improving the onset potential and Tafel slope determination of earth-abundant water oxidation electrocatalysts, Electrochim. Acta 388 (2021) 1–7.
[74] R. Vinodh, C. Deviprasath, C.V.V.M. Gopi, V.G.R. Kummara, R. Atchudan, T. Ahamad, H.J. Kim, M. Yi, Novel 13X Zeolite/PANI electrocatalyst for hydrogen and oxygen evolution reaction-sciencedirect, Int. J. Hydrog. Energy 45 (2020) 1–14.
[75] A. Alobaid, C. Wang, R.A. Adomaitis, Mechanism and kinetics of HER and OER on NiFe LDH films in an alkaline electrolyte, J. Electrochem. Soc. 165 (2018) J3395–J3404.
[76] S.A. Alkahtani, A.M. Mahmoud, M.H. Mahnashi, A.O. Alqarni, M.M. El-Wekil, Facile one pot sonochemical synthesis of layered nanostructure of ZnS NPs/rGO nanosheets for simultaneous analysis of daclatasvir and hydroxychloroquine, Microchem. J. 164 (2021) 972–980.
[77] X.Y. Wang, J.B. Le, Y. Fei, R.Q. Gao, M.X. Jing, W.Y. Yuan, C.M. Li, Self-assembled ultrasmall mixed Co-W phosphide nanoparticles on pristine graphene with remarkable synergistic effects as highly efficient electrocatalysts for hydrogen evolution, J. Mater. Chem. A 10 (2022) 7694–7704.